Cryo-EM structures and binding of mouse and human ACE2 to SARS-CoV-2 variants of concern indicate that mutations enabling immune escape could expand host range

Dongchun Ni[1], Priscilla Turelli[2], Bertrand Beckert[3], Sergey Nazarov[3], Emiko Uchikawa[3], Alexander Myasnikov[3], Florence Pojer[4], Didier Trono[2], Henning Stahlberg[1,$], Kelvin Lau[4,$]

[1]Laboratory of Biological Electron Microscopy (LBEM), Institute of Physics, School of Basic Science, École Polytechnique Fédérale de Lausanne (EPFL), and Dep. of Fund. Microbiology, Faculty of Biology and Medicine, University of Lausanne, Lausanne, Switzerland

[2]Laboratory of Virology and Genetics (LVG), School of Life Sciences, École polytechnique fédérale de Lausanne (EPFL), Lausanne, Switzerland

[3]Dubochet Center for Imaging (DCI), École polytechnique fédérale de Lausanne (EPFL) and University of Lausanne, Lausanne, Switzerland

[4]Protein Production and Structure Characterization Core Facility (PTPSP), School of Life Sciences, École polytechnique fédérale de Lausanne (EPFL), Lausanne, Switzerland

[$] Corresponding authors: henning.stahlberg@epfl.ch, kelvin.lau@epfl.ch

ABSTRACT

Investigation of potential hosts of the severe acute respiratory syndrome coronavirus-2 (SARS-CoV-2) is crucial to understanding future risks of spillover and spillback. SARS-CoV-2 has been reported to be transmitted from humans to various animals after requiring relatively few mutations.[1] There is significant interest in describing how the virus interacts with mice as they are well adapted to human environments, are used widely as infection models and can be infected.[2] Structural and binding data of the mouse ACE2 receptor with

the Spike protein of newly identified SARS-CoV-2 variants are needed to better understand the impact of immune system evading mutations present in variants of concern (VOC). Previous studies have developed mouse-adapted variants and identified residues critical for binding to heterologous ACE2 receptors.[3,4] Here we report the cryo-EM structures of mouse ACE2 bound to trimeric Spike ectodomains of four different VOC: Beta, Omicron BA.1, Omicron BA.2.12.1 and Omicron BA.4/5. These variants represent the oldest to the newest variants known to bind the mouse ACE2 receptor. Our high-resolution structural data complemented with bio-layer interferometry (BLI) binding assays reveal a requirement for a combination of mutations in the Spike protein that enable binding to the mouse ACE2 receptor.

AUTHOR SUMMARY

The SARS-CoV-2 virus can infect different types of animals beyond humans. The virus uses its Spike protein on its surface to bind to cells. These cells have a protein called ACE2 that the Spike protein recognizes. Animals have slightly different ACE2 receptors compared to humans. Mice are widely used as a research animal and live in the same environments as humans so scientists are particularly interested. Understanding how Spike proteins binds to the mouse ACE2 receptor allows us to understand the impact of immune evading mutations found in new variants. We use a high resolution imaging technique called cryo-electron microscopy to look at how different Spike variants bind to the ACE2 receptor from mouse at a resolution where we can see the amino acids. We can see directly the individual amino acids and mutations on the Spike protein that interact with the mouse ACE2 receptor. Many of the mutations found in variants of concern also increase the strength of binding to the mouse ACE2 receptor. This result suggests that mutations in the Spike protein of future

variants may have an additional effect in influencing how it binds to not only human ACE2 receptors but to mice and also different animals.

INTRODUCTION

Severe Acute Respiratory Syndrome (SARS) is a zoonotic disease caused by SARS-CoV infection, and its symptoms can range from mild to severe.[5] SARS-CoV was first identified in 2003 and it sparked a major global public health crisis.[6,7] Covid-19 is caused by SARS-CoV-2 infection, which was first reported in Wuhan in late 2019 and has led to a global pandemic.[8–10] Both viruses are of animal origin and their intermediate hosts prior to the jump to humans have not been precisely identified, however, it is accepted that like the SARS-CoV virus, the original host of the SARS-CoV-2 virus are most likely Rhinophilus bats .[11–14] It is well understood that angiotensin-converting enzyme 2 (ACE2) is a major receptor for host cell invasion by a range of coronaviruses, including SARS-CoV-2.[15–19] The Spike glycoprotein embedded in the viral envelope binds specifically to human or animal ACE2 on the cell surface, where it undergoes further membrane fusion and ultimately enters and infects the host cell. Due to the conserved nature of ACE2 in animals and constant selection of Spike variants, particularly ones that evade the human immune system, SARS-CoV-2 may exhibit a high degree of spillover and spillback.[20–22] Several animal infections or exposures have occurred during the covid-19 outbreak, including cats, dogs, rats, minks and American white-tailed deer.[23–26]

SARS-CoV-2 evades the human immune system in several ways, such as accumulating mutations on the Spike protein that reduce binding to host antibodies.[27–31] Significantly, many sites of mutations in VOC are located on the receptor binding domain (RBD) that

engages ACE2. Mutations that endow the ability for the Spike protein to evade antibodies in humans may also play an additional role by influencing ACE2 binding specificity and host range. The availability of 3D structures of variant RBDs interacting with the receptor is crucial for understanding how they continue to bind not only human ACE2 but potentially those of other animals. Indeed, there has been speculation and critical debate that the Omicron variant could have arisen in a mouse reservoir.[32–35] There have been structural studies of animal ACE2 receptors with the SARS-CoV-2 Spike protein but few focusing on mouse.[36–41] To better inform the relationship between these variants and potential species tropism, there is a need to examine the structural details between animal ACE2 receptors and the variant Spike proteins.

In this study, using cryo-electron microscopy single particle analysis (cryo-EM SPA) we resolved a series of high-resolution structures of the SARS-CoV-2 variant Spikes in complex with mouse ACE2, including the Beta, BA.1, BA.2.12.1 and BA.4/5 variants. We compared the binding affinity of different variants Spike to the receptors. We further analyzed the high-resolution structure of the widespread variant, BA.4/5, with human ACE2 using cryo-EM. Together, these suggest that there is a level of structural plasticity in the RBD of the Spike protein that is implicated in the evolution of both adaptation for animal hosts and immune escape.

RESULTS

Mouse ACE2 binds to Spike variants of concern Alpha, Beta, Gamma and Omicron subvariants

We performed a BLI binding screen between SARS-CoV-2 variants of concern Alpha, Beta and Gamma against a set of animal ACE2, including mouse ACE2 (mACE2), compared to

97 human ACE2 (hACE2). Interestingly, unlike cat, dog and mink ACE2 that could bind to the
98 wild-type Spike protein, mACE2 only showed a substantial binding signal against the VOC,
99 similar to other reports.[22,42,43] (S1 Fig) We decided to focus on and better characterize
100 mACE2 binding affinities against these Spike VOC and performed full BLI binding assays at
101 three concentrations. The wild-type Spike protein bound robustly hACE2 but not strongly to
102 mACE2, with only appreciable signal at the highest concentration of 300 nM (Fig 1). The
103 emergence of the N501Y mutation found in the receptor binding domain (RBD) of the Spike
104 protein of Alpha, Beta and Gamma variants (S2 Fig) has been associated with mice
105 susceptibility to infection.[44–47] In accordance with these results we found that Alpha, Beta
106 and Gamma Spikes had a higher affinity (K_d between 35, 45 and 25 nM, respectively) for
107 mACE2 compared to the ancestral Spike protein (K_d above 100nM) (Fig 1A). From the end
108 of 2021, Omicron strains have caused successive waves of infections worldwide.[48] While
109 affinity for hACE2 of Omicron BA.1 and BA.2 Spikes was 2.5 times increased compared to
110 the ancestral Spike, affinity for mACE2 was increased more than 40 times (Fig 1A). The
111 Spike protein from the more recent Omicron BA.2.12.1 and BA.4/5 variants, containing
112 respectively 1 and 3 mutations in the RBD compared to BA.2, retain a strong affinity for
113 mACE2 (Fig 1A and S2 Fig).

114 **Cryo-EM structure of Spike variants of concern bound to mouse ACE2 and BA.4/5 to**
115 **human ACE2**

116 To probe how variants of concern gained high affinity mACE2 binding we used cryo-EM to
117 determine the structures of trimeric Spike variants in complex with human and mouse ACE2
118 receptors. We used Spikes from Beta, Omicron BA.1, BA.2.12.1, and BA.4/5, and obtained
119 resolutions of 3.9 Å, 2.7Å, 2.9 Å and 2.9Å, respectively (Fig 2 and S3-S7 Figs). We also
120 solved the human ACE2/BA.4/5 Spike complex at 2.8Å for comparison (Fig 3). Our cryo-
121 EM structures determined with dimeric Fc-ACE2 and a trimerized Spike ectodomain

122 recapitulates the hACE2/wild-type complexes observed in other studies done by x-ray
123 crystallography (PDB 6M0J) or cryo-EM (PDB 7A94), with monomeric ACE2 and RBD or
124 monomeric ACE2 and trimerized Spike, respectively. All of our structures show that
125 mACE2/hACE2 bind the RBD of the Spike protein in the same manner at the binding
126 interface of a RBD in the up-position. The RBD is highly mobile and its transition between
127 the down- to its up- state reveals the ACE2 binding site and allows for it to bind ACE2. The
128 process is dynamic, and the proportion of RBD-down and -up has been shown to be
129 dependent on many factors such as mutations, glycans, pH and temperature.[49–56] During
130 cryo-EM data-processing we observed all the Spikes with a mixture of 2-up or 3-up
131 conformation, with each up-RBD having an ACE2 bound (S3-S7 Figs). To gain structural
132 information at side-chain level resolution of the binding interface, we performed image
133 processing of the cryo-EM data by location-focused refinement on an ACE2-bound RBD that
134 was the most well resolved. This yielded maps at higher quality for each variant's
135 ACE2/RBD interface, allowing us to better understand the effects of local mutations in these
136 regions (Figs 2B and 3 and S3-S8 Figs). Each of the mACE2/RBD complex structures were
137 highly superimposable, in particular the RBD domain and the two helices of mACE2 that
138 interact with it, with 0.5-0.8 Å RMSD compared to the mACE2/BA.1 complex (Fig 2C). The
139 hACE2/BA.4/5 complex is also highly superimposable with that of the crystal structure of the
140 isolated wildtype RBD in complex with monomeric hACE2 (PDB: 6M0J) with an RMSD of
141 0.9 Å and with movements principally at the ACE2 lobe distal to the interaction site with the
142 RBD (Fig 3B). The hACE2/BA.4/5 complex is very similar to the mACE2/BA.4/5 complex
143 with an overall RMSD of 0.6 Å (Fig 2D). We were also able to build most mutations and
144 residues present in the variants highlighting the high-quality of our cryo-EM reconstructions
145 (Fig 4 and S9 Fig).
146

147 **The combination of the N501Y and E484K mutation allow for Spike binding to mACE2**

148 The first mutation reported to be crucial for mACE2 engagement and shared by the Alpha,
149 Beta and Gamma and the more recent Omicron variants is the N501Y mutation. This
150 mutation is located within the RBD and is one residue that has been identified to enable
151 higher affinity interactions with the mACE2 receptor.[4,57,58] In the mACE2/Beta structure,
152 we observe that the Spike N501Y mutation which replaces a polar asparagine (N) residue
153 with a polar and aromatic tyrosine (Y) residue, allows for π-π interactions with Y41 of
154 mACE2, and enables a new cation-π and hydrogen bond interaction with histidine H353 of
155 mACE2 (Figs 1C and 4B). These new interactions stabilize the interface between mACE2
156 and the Beta RBD. Beta and Gamma both also share the E484K and K417N/T substitutions
157 in the Spike RBD (S2 Fig). These two residues are unfortunately not resolved in our cryo-EM
158 maps. However, *in vitro* BLI experiments showed that while the introduction of either
159 N501Y, K417N or the E484K mutations alone are not sufficient to confer binding to mACE2,
160 at the concentration of Spike protein tested here (75 nM), the combination of Y501 and K484
161 led to appreciable binding of the mutant Spike to mACE2 (S10 Fig).

162

163 **BA.1 mutations Q493R and Q498R further increase binding to mACE2**

164 We next investigated the impact of additional mutations found in Omicron variants BA.1,
165 BA.2, BA.2.12.1 and BA.4/5. These variants contain up to 34 mutations scattered across the
166 entire Spike protein, with the 15 of those concentrated on the RBD, including N501Y and
167 E484A (S2 Fig). In particular, some Omicron RBD mutations (K417N, G446S(BA.1),
168 E484A, F486S (BA.4/5) Q493R, G496S(BA.1), Q498R (BA.1, BA.2, BA.2.12.1) and
169 N501Y) have been shown to be associated with immune evasion, with a loss of antibody
170 binding or higher affinity ACE2 binding.[31,59–62] The accumulation of these mutations at
171 once prompted an ongoing discussion whether the Omicron variant may have arisen in a

172 chronically infected COVID-19 person who is immunocompromised, or possibly spilled over
173 from a mouse reservoir.[34] Indeed, the mACE2/BA.1 structure reveals multiple new
174 interactions localized in two different patches between the RBD and mACE2 (Fig 4A, B). In
175 patch 1, the longer arginine (R) sidechain of the BA.1 Q493R mutation allows for new
176 hydrogen bonds with mACE2 residues N31 and Q34. These were not possible with the
177 shorter glutamine (Q) residue present in the original Spike protein. In patch 2, Y501 is
178 observed to form cation-π interactions with H353 from mACE2, as in the mACE2/Beta
179 complex, and new BA.1 mutations G496S and Q498R form a new set of hydrogen bonds and
180 electrostatic interactions with mACE2's aspartic acid D38 (Fig 4B). This also reorients Y449
181 of the Omicron BA.1 RBD to form a new hydrogen bond with Q42 of mACE2. Furthermore,
182 mutation of Y505 to a smaller histidine residue now allows for better packing at the interface
183 and potentially a CH- π T-shape interaction.[63] Glutamate (E) 37 also flips away from the
184 interface and is now sandwiched between H353 and R393, stabilizing the overall
185 conformation of the interface. Overall, Omicron BA.1 mutations Q493R and Q498R form a
186 cascade of new interactions alongside the N501Y mutation present in preceding variants.
187 These additional contacts greatly increase the binding between mACE2 and Omicron Spike
188 proteins with measured affinities by BLI up to 14-20-fold stronger compared to Beta (Fig
189 1A). Interestingly, the BA.1 Q493R mutation eliminates a favorable interaction with the
190 human ACE2 residue K31 due to charge repulsion with R493 and thus is better adapted for
191 binding to mACE2 than to hACE2 (Fig 4B and S10 Fig).
192
193 **L452Q/R, F486V and the R493Q mutations of Omicron subvariants do not impact**
194 **mouse or human ACE2 binding**
195

196 Both the BA.2.12.1 and BA.4/5 Omicron subvariants carry the immune-evading L452Q/R
197 mutation first seen in the Delta variant (S2 Fig). The site of mutation is not within the RBD-
198 ACE2 binding interface and, as expected, the binding affinities for both hACE2 and mACE2
199 binding to BA.2.12.1 are unchanged compared to BA.2 (Fig 1A,B and S9 Fig). In the
200 mACE2/BA.2.12.1 structure, the critical interactions made by Spike residues R498 and Y501
201 with mACE2 within patch 2 are conserved as in BA.1 (Fig 4B). Surprisingly, compared to
202 BA.1, R493 of BA.2.12.1 forms an alternative hydrogen bonding network with mACE2
203 residues N31 and E35, instead of Q34, that now forms a new hydrogen bond with Y453 of
204 BA.2.12.1 suggesting a plasticity in its interactions (Fig 4B).
205
206 The Omicron subvariants BA.4 and BA.5 that were the principal variants during an infection
207 wave in the summer of 2022 also share the L452Q/R mutation. Additionally, BA.4 and BA.5
208 has gained an additional immunity evading F486V mutation, and the reversion of R493 back
209 to the wild-type Q493 (S2 Fig). The structure of the mACE2/BA.4/5 complex show crucial
210 changes at patch 1, where the BA.4/5 mutation F486V loses Van der Waals interactions with
211 adjacent mACE2 residues F83 and F28 compared to BA.1 (Fig 4B). Q493 on the Spike RBD
212 also no longer forms interactions with mACE2 due to the loss of the longer favorable
213 arginine side-chain.
214
215 It has been predicted by modelling and then demonstrated by deep mutation scans of the
216 RBD that the F486V mutation reduces the affinity of the RBD for hACE2 and before the
217 appearance of the BA.4/5 subvariant, mutation at this site was observed at very low
218 rates.[64,65] The hACE2/BA.4/5 complex confirms this loss of hydrophobic contacts for
219 F486V mutation with hACE2 residues F28 and Y83, as seen with mACE2/BA.4/5, however,
220 Q493 now reestablishes a hydrogen bond interaction with hACE2 K31 residue, an interaction

221 previously first lost with the appearance of the Omicron lineage due to the charge repulsion
222 between R498 and K31 (Fig 4C and S10 Fig). The combination of these two mutations
223 allows for the BA.4/5 Spike to maintain high affinity interactions with both hACE2 and
224 mACE2. This is an example of the interplay between balancing immune evasion, while
225 maintaining high-affinity receptor binding. The other principal interactions between mACE2
226 and Spike's BA.4/5 in patch 2 are comparable to those observed between mACE2 and
227 Omicron subvariants BA.1 or BA2.12.1.
228
229 **DISCUSSION**
230 New variants of the SARS-CoV-2 virus have emerged posing a challenge to vaccine/antibody
231 efficacy and global pandemic management. We report here that since the appearance of the
232 first variant of concern Alpha, the SARS-CoV-2 Spike glycoprotein has serendipitously
233 gained the ability to also bind the mouse ACE2 receptor potentially broadening its host
234 range.[44–47] Here we demonstrate by a structural approach that this ability to bind the
235 mouse ACE2 receptor has further been maintained even with immune evading mutations in
236 the Omicron lineage.
237
238 Our BLI assays with early variants of concern and mutants agree with earlier findings that
239 N501Y and E484K are critical residues that allow for the Spike protein to bind to other
240 mammalian ACE2 homologs. To our knowledge, there has been no reported structure of the
241 Beta Spike bound to a non-human ACE2. Our cryo-EM structure illuminates how a single
242 mutation, N501Y, allows for new interactions especially with the mACE2-unique residue
243 H353 via cation- π interactions, analogous to K353 as observed with Alpha, Beta and Gamma
244 Spike bound hACE2.[66].
245

246 With the appearance of the Omicron variant and its subvariants, many epitopes on the surface
247 of the Spike glycoprotein have mutated leading to reduced or abolished antibody binding.
248 The BA.1 variant was first reported with increased resistance to antibodies and significantly
249 stronger binding to hACE2.[59,67] We also observe that mACE2 also shows drastically
250 increased binding (almost 10-fold) to the Omicron BA.1 Spike compared to all other variants
251 that preceded it. The cryo-EM structure of mACE2/BA.1 reveals residues on the Spike
252 protein that increase the number of interactions with mACE2: N501Y, Q493R, G496S and
253 Q498R. This structural observation is consistent with literature reports that reported Spike
254 mutations N501Y, Q493H and K417N increases binding to ACE2 from mice and other
255 species.[3,4,68] We further observe that Spike proteins from Omicron subvariants with
256 significant antibody evasion abilities such as BA.2.12.1 and BA.4/5 still bind to mACE2
257 demonstrating that the SARS-CoV-2 virus can balance both evasion of the human humoral
258 immune response and its ability to bind to different host species. Notably, this is highlighted
259 at position 493, where in the BA.1 Spike, the glutamine (Q) to arginine (R) mutation allows
260 for new hydrogen bonds with mACE2 residues. However, in humans, it has been shown that
261 this position favored antibody evasion at the cost of an interaction with hACE2 residue K31.
262 Further Omicron subvariants such as BA.4/5 have reverted the arginine back to glutamine
263 while picking up the F486V mutation that reduces van der Waals at the ACE2 binding
264 interface. This compensatory mechanism allowed for further immune evasion while
265 maintaining adequate binding affinity for the hACE2 Spike. Importantly, binding to mACE2
266 was unaffected even with the loss of two interactions.
267
268 Our structural study of human and mouse ACE2 bound to variant Spikes is not without
269 limitations. The ability to bind mACE2 does not necessarily imply that it is able to infect and
270 replicate in mouse.[69] However, numerous *in vivo* mouse studies with early-pandemic,

271 Omicron and mouse-adapted variants demonstrate that these variants are able to infect and
272 cause disease[35,44,45,57,70] In particular, our cryo-EM models shed light on the structural
273 basis of mACE2 binding to these variants. Importantly, our data complements previous
274 studies that also identified mutations that enable mACE2 binding, such as N501Y.
275
276 In summary, our structural data and binding analysis of mACE2 to SARS-CoV-2 variants of
277 concern highlight how mutations acquired to evade the immune response in humans may
278 have an impact on the binding to ACE2 receptors of other species thus possibly increasing
279 host susceptibility. Our binding assays and structural analysis identified 4 of the mutations
280 found in SARS-CoV-2 Spikes and known to be associated with immune escape, N501Y,
281 E484A, Q493R and Q498R, as critical mutations involved in high-affinity binding of VOC
282 Spikes to the mouse ACE2 receptor, and as such potentially allowing for expansion of SARS-
283 CoV-2 host range.
284
285 **FIGURE LEGENDS**
286 **Fig 1**. **mACE2 and hACE2 binding to variants of concern. (A)** BLI binding assays of
287 captured dimeric mouse ACE2 versus various concentrations of Spike variants of concern.
288 Data curves are colored by concentration and the black line indicates the 1:1 fit of the data.
289 **(B)** BLI binding assays of captured dimeric human ACE2 versus various concentrations of
290 Spike variants of concern. Data curves are colored by concentration and the black line
291 indicates the 1:1 fit of the data. **c.** Sequence alignment of human ACE2 with mouse ACE2
292 and other selected species. Red boxes highlight critical differences between human and
293 mouse ACE2 residues.
294 **Fig 2**. **Cryo-EM structures of mACE2 bound to variants of concern**

295 **(A)** Cryo-EM densities of the full mACE2/Spike variant of concern complexes. Each
296 protomer of the Spike trimer is colored separately with mACE2 colored in grey. **(B)** Focused
297 refinement of the RBD-mACE2 interface of each complex as in (A). **(C)** Superposition of
298 RBD-mACE2 complexes on to the BA.1-mACE2 complex show mACE2 binds similarly for
299 all variants. **(D)** Superposition of the BA.4/5 RBD-hACE2 complex with the BA.4/5 RBD-
300 mACE2 complex.
301
302 **Fig 3**. **Cryo-EM structures of hACE2 bound to the BA.4/5 Spike**
303 **(A)** Cryo-EM densities of the full hACE2/BA.4/5 Spike. Each protomer of the Spike trimer is
304 colored separately with hACE2 colored in light green. Inset shows focused refinement of the
305 RBD-hACE2 interface. **(B)** Superposition of BA.4/5 RBD-hACE2 complex with the BA.1
306 RBD-hACE2 complex (PDB 7T9L).
307
308 **Fig** 4. **Structural basis of mACE2 binding to variants of concern and of hACE2/BA.4/5**
309 **(A)** Zoomed view of the binding interface between mACE2 and RBD of variants of concern
310 with cryo-EM densities. **(B)** Highlighted views of specific interaction sites of patch 1 and
311 patch 2 as indicated in (A). **(C)** Zoomed view of the binding interface between hACE2 and
312 RBD of variants of concern with cryo-EM densities with highlighted views of specific
313 interaction sites.
314
315
316 **DATA AVAILABILITY**
317 Cryo-EM maps for the Spike variants in complex with mouse ACE2 were deposited in the
318 Electron Microscopy Data Bank (EMDB) under the access codes EMD-15541 (full map,
319 Beta, two mACE2 bound), EMD-15589 (local map, mACE2/Beta), EMD- 15580 (full map,

320 BA.1, two mACE2 bound), EMD-15581 (full map, BA.1, three mACE2 bound), EMD-15590
321 (local map, mACE2/BA.1), EMD-15584 (full map, BA.2.12.1, two mACE2 bound), EMD-
322 15585 (full map, BA2.12.1, three mACE2 bound), EMD-15591 (local map,
323 mACE2/BA.2.12.1), EMD-15586 (full map, BA.4/5, two mACE2 bound) and EMD-15592
324 (local map, mACE2/BA.4/5).
325
326 Maps for Spike the human ACE2/Omicron BA.4/5 complex were deposited in the EMDB
327 under the access codes EMD-15587 (full map, BA.4/5, three hACE2 bound) and EMD-15588
328 (local map, hACE2/BA.4/5).
329
330 Atomic models were deposited in Protein Data Bank (PDB) under the access codes of PDB-
331 8AQS (hACE2-BA.4/5), PDB-8AQT (mACE2/Beta), PDB-8AQU (mACE2/BA.1), PDB-
332 8AQV (mACE2/BA.2.12.1) and PDB-8AQW (mACE2/BA.4/5).
333
334 Raw electron microscopy image data were deposited at the Electron Microscopy Public
335 Image Archive (EMPIAR) under access codes EMPIAR-11181 (mACE2/Beta), EMPIAR-
336 11179 (mACE2/BA.1), EMPIAR-11180 (mACE2/BA.2.12.1), EMPIAR-11177
337 (mACE2/BA.4/5), EMPIAR-11176 (hACE2/BA.4/5).
338
339 **CONTRIBUTIONS**
340 D.N., K.L., P.T., F.P., D.T. designed the project. P.T. designed and cloned the Spike variants.
341 K.L purified the Omicron Spike and ACE2 and performed BLI assays. B.B., S.N., E.U.,
342 A.M., froze and screened cryo-EM grids, collected data, and performed on-the-fly
343 processing. D.N. processed cryo-EM data and built models. D.N. and K.L. analyzed data and

344 prepared figures. K.L., D.N., wrote the manuscript and P.T. contributed to the editing of the
345 manuscript. F.P., H.S., and D.T. supervised the project.
346

347 **ACKNOWLEDGEMENTS**
348 Cryo-EM data collection and initial image processing was performed at the Dubochet Center
349 for Imaging, a common initiative of the EPFL, UNIL and UNIGE, with data collection
350 performed in both Geneva and Lausanne. We thank Yashar Sadian for data collection on the
351 Talos Arctica. We thank Rosa Schier, Laurence Durrer, Soraya Quinche and Michael
352 François of the Protein Production and Structure Core Facility of EPFL for helping in the
353 production of Spike Omicron and ACE2 and Charlene Raclot for cloning of the Spike
354 variants. This work was supported in part by NCCR TransCure, a National Centre of
355 Competence in Research, funded by the Swiss National Science Foundation (grant number
356 185544)
357

358 **METHODS AND MATERIALS**

359 **Protein Production and Purification**

360 The Spike trimer was designed to mimic the native trimeric conformation of the protein in vivo
361 and the expression vector was kindly provided by Prof. Jason McLellan, University of Texas,
362 Austin (TX), USA. It encoded the prefusion ectodomain of the original 2019-CoV Spike,
363 containing a native signal peptide, residues 986 and 987 mutated to proline (2P), a mutated
364 putative furin cleavage site (residues 682-685 mutated to GSAS), a C-terminal T4 foldon fusion
365 domain to stabilize the trimer complex, followed by C-terminal 8x His and 2x Strep tags for
366 affinity purification.[19] The trimeric Spike protein was expressed as previously reported.[71–
367 73] transiently expressed in suspension-adapted ExpiCHO cells (Thermo Fisher) in ProCHO5
368 medium (Lonza) at 5 x10^6 cells/mL using PEI MAX (Polysciences) for DNA delivery. At 1 h

369 post-transfection, dimethyl sulfoxide (DMSO; AppliChem) was added to 2% (v/v). Following
370 a 7-day incubation with agitation at 31 °C and 4.5% CO_2, the cell culture medium was
371 harvested and clarified using a 0.22 µm filter. The conditioned medium was loaded onto
372 Streptactin XT columns (IBA) washed with PBS and eluted with 50 mM biotin in 150 mM
373 NaCl, 100 mM HEPES 7.5. Eluted protein was then dialyzed overnight into PBS. The purity
374 of Spike trimers was determined to be >99% pure by SDS-PAGE analysis. Point mutations
375 were generated by InFusion-mediated site directed mutagenesis. Variant clones were generated
376 by gene synthesis (Twist Biosciences, Genscript and IDT) on the 2019-CoV Spike background
377 as above. All mutants were produced and purified in an identical manner to the original 2019-
378 Cov S protein.
379
380 **Cryo-electron microscopy**
381 **mACE2/Beta complex**
382
383 Cryo-EM grids were prepared with a Leica EM GP2 (Leica) plunge-freezing device, using
384 Quantifoil R2/1 copper 400 grids. 3.0 µL of a sample containing 0.4 µM Beta Spike and 0.7
385 µM mACE2-Fc was applied to the glow-discharged grids, and backblotted for 2 s with a 10 s
386 wait time, 80% humidity and 10 °C in the sample chamber, and the blotted grids were
387 plunge-frozen in liquid nitrogen-cooled liquid ethane.
388
389 Grids were screened for particle presence and ice quality on a TFS Talos Arctica transmission
390 electron microscope (TEM) operated at 200kV. Cryo-EM data was collected using the same
391 microscope, equipped with a TFS Falcon 3 camera. Movies were recorded at a nominal
392 magnification of 150kx, corresponding to a 0.9759Å pixel, with defocus values ranging from

393 -0.8 to -2.5 µm. Exposures were adjusted automatically to 40 e-/Å2 total dose with automatic
394 collection using EPU.
395
396 **mACE2/Omicron BA.1 complex**
397 Cryo-EM grids were prepared with a Vitrobot Mark IV (Thermofisher Scientific (TFS)).
398 Quantifoil R1.2/1.3 Au 400 holey carbon grids were glow-discharged for 120 s at 15mA
399 using a PELCO easiGlow device (Ted Pella, Inc.). 3.0 µL of a sample containing 9 µM
400 Omicron BA.1 and 16 µM mACE-Fc was applied to the glow-discharged grids, and blotted
401 for 6 s under blot force 10 at 100% humidity and 4 °C in the sample chamber, and the blotted
402 grids were plunge-frozen in liquid nitrogen-cooled liquid ethane.
403
404 Grids were screened for particle presence and ice quality on a TFS Glacios TEM (200kV),
405 and the best grids were transferred to TFS Titan Krios G4 TEM. Cryo-EM data was collected
406 using TFS Titan Krios G4, equipped with a Cold-FEG and Selectris X energy filter, on a
407 Falcon IV detector in electron counting mode. Falcon IV gain references were collected just
408 before data collection. Data was collected using TFS EPU v2.12.1 using aberration-free
409 image shift protocol (AFIS). Movies were recorded at the nominal magnification of 165kx,
410 corresponding to the 0.726Å pixel size at the specimen level, with defocus values ranging
411 from -0.7 to -2.0 µm. Exposures were adjusted automatically to 60 e-/$Å^2$ total dose.
412
413 **hACE2/Omicron BA.4/5, mACE2/Omicron BA.4/5, mACE2/Omicron BA.2.12.1**
414
415 Cryo-EM grids were prepared with a Vitrobot Mark IV (Thermofisher Scientific (TFS)).
416 Quantifoil R1.2/1.3 Au 400 holey carbon grids were glow-discharged for 120 s at 15mA
417 using a PELCO easiGlow device (Ted Pella, Inc.). 3.0 µL of a sample containing 14 µM of

418 the corresponding Spike and 25 μM ACE-Fc was applied to the glow-discharged grids, and
419 blotted for 6 s under blot force 10 at 100% humidity and 4 °C in the sample chamber, and the
420 blotted grid was plunge-frozen in liquid nitrogen-cooled liquid ethane.
421
422 Grids were screened for particle presence and ice quality on a TFS Glacios TEM (200kV),
423 and the best grids were transferred to TFS Titan Krios G4 TEM. Cryo-EM data was collected
424 using the TFS Titan Krios G4 TEM, equipped with a Cold-FEG, on a Falcon IV detector in
425 electron counting mode. Falcon IV gain references were collected just before data collection.
426 Data was collected using TFS EPU v2.12.1 using aberration-free image shift protocol (AFIS).
427 Movies were recorded at nominal magnification of 165kx, corresponding to the 0.83Å pixel
428 size at the specimen level, with defocus values ranging from -0.7 to -2.5 μm. Exposures were
429 adjusted automatically to 60 e-/Å2 total dose.
430
431 **Cryo-EM image processing**
432 On-the-fly processing was first performed during data acquisition for evaluating the data
433 quality during screening by using cryoSPARC live v3.3.1.4.[74] The obtained ab-initio
434 structures were used as templates for better particle picking. Motion correction was
435 performed on raw stacks without binning, using the cryoSPARC implementation of motion
436 correction. The full data processing workflow is shown in Supplementary information, S3-S8
437 Figs and processing statistics on S1 Table.
438
439 **Cryo-electron microscopy model building**
440 The models of a SARS-CoV2 Spike (PDB ID 7QO7), mouse ACE2 (PDB ID 7FDK) and
441 human ACE2 (PDB ID 7FDG) were re-fit into the cryo-EM maps with UCSF Chimera.[75]
442 These docked models were extended and rebuilt manually with refinement, using Coot and

443 Phenix. Statistics reported on S1 Table are from MolProbity as implemented in Phenix real-
444 space refine.[76,77] Figures were prepared in UCSF ChimeraX.[78]
445
446 **Biolayer Interferometry (BLI)**
447 All experiments were performed on a Gator BLI system. Running buffer was 150 mM NaCl,
448 10 mM HEPES 7.5. For binding assays, dimeric Fc-ACE2 was diluted to 10 µg/mL and
449 captured with MFc tips (GatorBio). Loaded tips were dipped into a 3 or 2-fold serial dilution
450 series (300 nM, 100 nM, 33.3 nM, or 100 nM, 50 nM, 25 nM) of target analyte Spike protein.
451 Screening of independent point mutations was done as above at a single concentration of 75
452 nM. Curves were processed using the Gator software with a 1:1 fit after background
453 subtraction. Plots were generated in Prism 9. Original data is provided in an excel spreadsheet
454 as S1 Dataset.
455
456 **REFERENCES**

457 1. Tan CCS, Lam SD, Richard D, Owen CJ, Berchtold D, Orengo C, et al. Transmission of
458 SARS-CoV-2 from humans to animals and potential host adaptation. Nat Commun.
459 2022;13: 2988. doi:10.1038/s41467-022-30698-6

460 2. Muñoz-Fontela C, Widerspick L, Albrecht RA, Beer M, Carroll MW, Wit E de, et al.
461 Advances and gaps in SARS-CoV-2 infection models. PLOS Pathogens. 2022;18:
462 e1010161. doi:10.1371/journal.ppat.1010161

463 3. Sun S, Gu H, Cao L, Chen Q, Ye Q, Yang G, et al. Characterization and structural basis of a
464 lethal mouse-adapted SARS-CoV-2. Nat Commun. 2021;12: 5654. doi:10.1038/s41467-
465 021-25903-x

466 4. Dinnon KH, Leist SR, Schäfer A, Edwards CE, Martinez DR, Montgomery SA, et al. A
467 mouse-adapted model of SARS-CoV-2 to test COVID-19 countermeasures. Nature.
468 2020;586: 560–566. doi:10.1038/s41586-020-2708-8

469 5. Fischhoff IR, Castellanos AA, Rodrigues JPGLM, Varsani A, Han BA. Predicting the
470 zoonotic capacity of mammals to transmit SARS-CoV-2. Proceedings of the Royal
471 Society B: Biological Sciences. 2021;288: 20211651. doi:10.1098/rspb.2021.1651

472 6. Cherry JD, Krogstad P. SARS: The First Pandemic of the 21st Century. Pediatr Res.
473 2004;56: 1–5. doi:10.1203/01.PDR.0000129184.87042.FC

474 7. Yang Y, Peng F, Wang R, Guan K, Jiang T, Xu G, et al. The deadly coronaviruses: The 2003
475 SARS pandemic and the 2020 novel coronavirus epidemic in China. Journal of
476 Autoimmunity. 2020;109: 102434. doi:10.1016/j.jaut.2020.102434

477 8. Fauci AS, Lane HC, Redfield RR. Covid-19 — Navigating the Uncharted. New England
478 Journal of Medicine. 2020;382: 1268–1269. doi:10.1056/NEJMe2002387

479 9. Zhou P, Yang X-L, Wang X-G, Hu B, Zhang L, Zhang W, et al. A pneumonia outbreak
480 associated with a new coronavirus of probable bat origin. Nature. 2020;579: 270–273.
481 doi:10.1038/s41586-020-2012-7

482 10. Wu F, Zhao S, Yu B, Chen Y-M, Wang W, Song Z-G, et al. A new coronavirus associated
483 with human respiratory disease in China. Nature. 2020;579: 265–269.
484 doi:10.1038/s41586-020-2008-3

485 11. Shi Z, Hu Z. A review of studies on animal reservoirs of the SARS coronavirus. Virus
486 Research. 2008;133: 74–87. doi:10.1016/j.virusres.2007.03.012

487 12. Temmam S, Vongphayloth K, Baquero E, Munier S, Bonomi M, Regnault B, et al. Bat
488 coronaviruses related to SARS-CoV-2 and infectious for human cells. Nature. 2022;604:
489 330–336. doi:10.1038/s41586-022-04532-4

490 13. Lytras S, Xia W, Hughes J, Jiang X, Robertson DL. The animal origin of SARS-CoV-2.
491 Science. 2021;373: 968–970. doi:10.1126/science.abh0117

492 14. Hu B, Guo H, Zhou P, Shi Z-L. Characteristics of SARS-CoV-2 and COVID-19. Nat Rev
493 Microbiol. 2021;19: 141–154. doi:10.1038/s41579-020-00459-7

494 15. Ge X-Y, Li J-L, Yang X-L, Chmura AA, Zhu G, Epstein JH, et al. Isolation and
495 characterization of a bat SARS-like coronavirus that uses the ACE2 receptor. Nature.
496 2013;503: 535–538. doi:10.1038/nature12711

497 16. Walls AC, Tortorici MA, Frenz B, Snijder J, Li W, Rey FA, et al. Glycan shield and epitope
498 masking of a coronavirus spike protein observed by cryo-electron microscopy. Nat
499 Struct Mol Biol. 2016;23: 899–905. doi:10.1038/nsmb.3293

500 17. Walls AC, Park Y-J, Tortorici MA, Wall A, McGuire AT, Veesler D. Structure, Function, and
501 Antigenicity of the SARS-CoV-2 Spike Glycoprotein. Cell. 2020;181: 281-292.e6.
502 doi:10.1016/j.cell.2020.02.058

503 18. Li W, Moore MJ, Vasilieva N, Sui J, Wong SK, Berne MA, et al. Angiotensin-converting
504 enzyme 2 is a functional receptor for the SARS coronavirus. Nature. 2003;426: 450–
505 454. doi:10.1038/nature02145

506 19. Wrapp D, Wang N, Corbett KS, Goldsmith JA, Hsieh C-L, Abiona O, et al. Cryo-EM
507 structure of the 2019-nCoV spike in the prefusion conformation. Science. 2020 [cited
508 19 Feb 2020]. doi:10.1126/science.abb2507

509 20. Damas J, Hughes GM, Keough KC, Painter CA, Persky NS, Corbo M, et al. Broad host
510 range of SARS-CoV-2 predicted by comparative and structural analysis of ACE2 in
511 vertebrates. Proceedings of the National Academy of Sciences. 2020;117: 22311–
512 22322. doi:10.1073/pnas.2010146117

513 21. Liu Y, Hu G, Wang Y, Ren W, Zhao X, Ji F, et al. Functional and genetic analysis of viral
514 receptor ACE2 orthologs reveals a broad potential host range of SARS-CoV-2.
515 Proceedings of the National Academy of Sciences. 2021;118: e2025373118.
516 doi:10.1073/pnas.2025373118

517 22. Conceicao C, Thakur N, Human S, Kelly JT, Logan L, Bialy D, et al. The SARS-CoV-2 Spike
518 protein has a broad tropism for mammalian ACE2 proteins. PLOS Biology. 2020;18:
519 e3001016. doi:10.1371/journal.pbio.3001016

520 23. Shi J, Wen Z, Zhong G, Yang H, Wang C, Huang B, et al. Susceptibility of ferrets, cats,
521 dogs, and other domesticated animals to SARS–coronavirus 2. Science. 2020;368:
522 1016–1020. doi:10.1126/science.abb7015

523 24. Oude Munnink BB, Sikkema RS, Nieuwenhuijse DF, Molenaar RJ, Munger E, Molenkamp
524 R, et al. Transmission of SARS-CoV-2 on mink farms between humans and mink and
525 back to humans. Science. 2021;371: 172–177. doi:10.1126/science.abe5901

526 25. Palmer MV, Martins M, Falkenberg S, Buckley A, Caserta LC, Mitchell PK, et al.
527 Susceptibility of White-Tailed Deer (Odocoileus virginianus) to SARS-CoV-2. Journal of
528 Virology. 2021;95: e00083-21. doi:10.1128/JVI.00083-21

529 26. Bao L, Deng W, Huang B, Gao H, Liu J, Ren L, et al. The pathogenicity of SARS-CoV-2 in
530 hACE2 transgenic mice. Nature. 2020;583: 830–833. doi:10.1038/s41586-020-2312-y

531 27. Mlcochova P, Kemp SA, Dhar MS, Papa G, Meng B, Ferreira IATM, et al. SARS-CoV-2
532 B.1.617.2 Delta variant replication and immune evasion. Nature. 2021;599: 114–119.
533 doi:10.1038/s41586-021-03944-y

534 28. McCallum M, Bassi J, De Marco A, Chen A, Walls AC, Di Iulio J, et al. SARS-CoV-2 immune
535 evasion by the B.1.427/B.1.429 variant of concern. Science. 2021;373: 648–654.
536 doi:10.1126/science.abi7994

537 29. Harvey WT, Carabelli AM, Jackson B, Gupta RK, Thomson EC, Harrison EM, et al. SARS-
538 CoV-2 variants, spike mutations and immune escape. Nat Rev Microbiol. 2021;19: 409–
539 424. doi:10.1038/s41579-021-00573-0

540 30. Hu J, Peng P, Cao X, Wu K, Chen J, Wang K, et al. Increased immune escape of the new
541 SARS-CoV-2 variant of concern Omicron. Cell Mol Immunol. 2022;19: 293–295.
542 doi:10.1038/s41423-021-00836-z

543 31. Cao Y, Yisimayi A, Jian F, Song W, Xiao T, Wang L, et al. BA.2.12.1, BA.4 and BA.5 escape
544 antibodies elicited by Omicron infection. Nature. 2022; 1–10. doi:10.1038/s41586-022-
545 04980-y

546 32. Bashor L, Gagne RB, Bosco-Lauth AM, Bowen RA, Stenglein M, VandeWoude S. SARS-
547 CoV-2 evolution in animals suggests mechanisms for rapid variant selection.
548 Proceedings of the National Academy of Sciences. 2021;118: e2105253118.
549 doi:10.1073/pnas.2105253118

550 33. Kim Y, Gaudreault NN, Meekins DA, Perera KD, Bold D, Trujillo JD, et al. Effects of Spike
551 Mutations in SARS-CoV-2 Variants of Concern on Human or Animal ACE2-Mediated
552 Virus Entry and Neutralization. Microbiology Spectrum. 2022;10: e01789-21.
553 doi:10.1128/spectrum.01789-21

554 34. Wei C, Shan K-J, Wang W, Zhang S, Huan Q, Qian W. Evidence for a mouse origin of the
555 SARS-CoV-2 Omicron variant. Journal of Genetics and Genomics. 2021 [cited 5 Jan
556 2022]. doi:10.1016/j.jgg.2021.12.003

557 35. Halfmann PJ, Iida S, Iwatsuki-Horimoto K, Maemura T, Kiso M, Scheaffer SM, et al. SARS-
558 CoV-2 Omicron virus causes attenuated disease in mice and hamsters. Nature. 2022; 1–
559 1. doi:10.1038/s41586-022-04441-6

560 36. Wu L, Chen Q, Liu K, Wang J, Han P, Zhang Y, et al. Broad host range of SARS-CoV-2 and
561 the molecular basis for SARS-CoV-2 binding to cat ACE2. Cell Discovery. 2020;6: 1–12.
562 doi:10.1038/s41421-020-00210-9

563 37. Xu Y, Wu C, Cao X, Gu C, Liu H, Jiang M, et al. Structural and biochemical mechanism for
564 increased infectivity and immune evasion of Omicron BA.2 variant compared to BA.1
565 and their possible mouse origins. Cell Res. 2022;32: 609–620. doi:10.1038/s41422-022-
566 00672-4

567 38. Su C, He J, Han P, Bai B, Li D, Cao J, et al. Molecular Basis of Mink ACE2 Binding to SARS-
568 CoV-2 and Its Mink-Derived Variants. Journal of Virology. 2022;96: e00814-22.
569 doi:10.1128/jvi.00814-22

570 39. Lan J, Chen P, Liu W, Ren W, Zhang L, Ding Q, et al. Structural insights into the binding of
571 SARS-CoV-2, SARS-CoV, and hCoV-NL63 spike receptor-binding domain to horse ACE2.
572 Structure. 2022;30: 1432-1442.e4. doi:10.1016/j.str.2022.07.005

573 40. Li S, Yang R, Zhang D, Han P, Xu Z, Chen Q, et al. Cross-species recognition and molecular
574 basis of SARS-CoV-2 and SARS-CoV binding to ACE2s of marine animals. National
575 Science Review. 2022;9: nwac122. doi:10.1093/nsr/nwac122

576 41. Liu K, Tan S, Niu S, Wang J, Wu L, Sun H, et al. Cross-species recognition of SARS-CoV-2
577 to bat ACE2. PNAS. 2021;118. doi:10.1073/pnas.2020216118

578 42. Li Y, Wang H, Tang X, Fang S, Ma D, Du C, et al. SARS-CoV-2 and Three Related
579 Coronaviruses Utilize Multiple ACE2 Orthologs and Are Potently Blocked by an
580 Improved ACE2-Ig. Journal of Virology. 2020;94: e01283-20. doi:10.1128/JVI.01283-20

581 43. Zhao X, Chen D, Szabla R, Zheng M, Li G, Du P, et al. Broad and Differential Animal
582 Angiotensin-Converting Enzyme 2 Receptor Usage by SARS-CoV-2. Journal of Virology.
583 2020;94. doi:10.1128/JVI.00940-20

584 44. Montagutelli X, Prot M, Levillayer L, Salazar EB, Jouvion G, Conquet L, et al. The B1.351
585 and P.1 variants extend SARS-CoV-2 host range to mice. Microbiology; 2021 Mar.
586 doi:10.1101/2021.03.18.436013

587 45. Pan T, Chen R, He X, Yuan Y, Deng X, Li R, et al. Infection of wild-type mice by SARS-CoV-
588 2 B.1.351 variant indicates a possible novel cross-species transmission route. Sig
589 Transduct Target Ther. 2021;6: 1–12. doi:10.1038/s41392-021-00848-1

590 46. Thakur N, Gallo G, Newman J, Peacock TP, Biasetti L, Hall CN, et al. SARS-CoV-2 variants
591 of concern alpha, beta, gamma and delta have extended ACE2 receptor host ranges.
592 Journal of General Virology. 103: 001735. doi:10.1099/jgv.0.001735

593 47. Yao W, Wang Y, Ma D, Tang X, Wang H, Li C, et al. Circulating SARS-CoV-2 variants
594 B.1.1.7, 501Y.V2, and P.1 have gained ability to utilize rat and mouse Ace2 and altered
595 in vitro sensitivity to neutralizing antibodies and ACE2-Ig. bioRxiv. 2021;
596 2021.01.27.428353. doi:10.1101/2021.01.27.428353

597 48. Tegally H, Moir M, Everatt J, Giovanetti M, Scheepers C, Wilkinson E, et al. Emergence of
598 SARS-CoV-2 Omicron lineages BA.4 and BA.5 in South Africa. Nat Med. 2022; 1–6.
599 doi:10.1038/s41591-022-01911-2

600 49. Cai Y, Zhang J, Xiao T, Lavine CL, Rawson S, Peng H, et al. Structural basis for enhanced
601 infectivity and immune evasion of SARS-CoV-2 variants. Science. 2021;373: 642–648.
602 doi:10.1126/science.abi9745

603 50. Wang Y, Xu C, Wang Y, Hong Q, Zhang C, Li Z, et al. Conformational dynamics of the Beta
604 and Kappa SARS-CoV-2 spike proteins and their complexes with ACE2 receptor
605 revealed by cryo-EM. Nat Commun. 2021;12: 7345. doi:10.1038/s41467-021-27350-0

606 51. Gobeil SM-C, Janowska K, McDowell S, Mansouri K, Parks R, Manne K, et al. D614G
607 Mutation Alters SARS-CoV-2 Spike Conformation and Enhances Protease Cleavage at
608 the S1/S2 Junction. Cell Reports. 2021;34. doi:10.1016/j.celrep.2020.108630

609 52. Zhao Z, Zhou J, Tian M, Huang M, Liu S, Xie Y, et al. Omicron SARS-CoV-2 mutations
610 stabilize spike up-RBD conformation and lead to a non-RBM-binding monoclonal
611 antibody escape. Nat Commun. 2022;13: 4958. doi:10.1038/s41467-022-32665-7

612 53. Sztain T, Ahn S-H, Bogetti AT, Casalino L, Goldsmith JA, Seitz E, et al. A glycan gate
613 controls opening of the SARS-CoV-2 spike protein. Nat Chem. 2021;13: 963–968.
614 doi:10.1038/s41557-021-00758-3

615 54. Pang YT, Acharya A, Lynch DL, Pavlova A, Gumbart JC. SARS-CoV-2 spike opening
616 dynamics and energetics reveal the individual roles of glycans and their collective
617 impact. Commun Biol. 2022;5: 1–11. doi:10.1038/s42003-022-04138-6

618 55. Zhou T, Tsybovsky Y, Gorman J, Rapp M, Cerutti G, Chuang G-Y, et al. Cryo-EM Structures
619 of SARS-CoV-2 Spike without and with ACE2 Reveal a pH-Dependent Switch to Mediate
620 Endosomal Positioning of Receptor-Binding Domains. Cell Host & Microbe. 2020;28:
621 867-879.e5. doi:10.1016/j.chom.2020.11.004

622 56. Edwards RJ, Mansouri K, Stalls V, Manne K, Watts B, Parks R, et al. Cold sensitivity of the
623 SARS-CoV-2 spike ectodomain. Nature Structural & Molecular Biology. 2021; 1–4.
624 doi:10.1038/s41594-020-00547-5

625 57. Rathnasinghe R, Jangra S, Ye C, Cupic A, Singh G, Martínez-Romero C, et al.
626 Characterization of SARS-CoV-2 Spike mutations important for infection of mice and
627 escape from human immune sera. Nat Commun. 2022;13: 3921. doi:10.1038/s41467-
628 022-30763-0

629 58. Starr TN, Zepeda SK, Walls AC, Greaney AJ, Alkhovsky S, Veesler D, et al. ACE2 binding is
630 an ancestral and evolvable trait of sarbecoviruses. Nature. 2022;603: 913–918.
631 doi:10.1038/s41586-022-04464-z

632 59. McCallum M, Czudnochowski N, Rosen LE, Zepeda SK, Bowen JE, Walls AC, et al.
633 Structural basis of SARS-CoV-2 Omicron immune evasion and receptor engagement.
634 Science. 2022;375: 864–868. doi:10.1126/science.abn8652

635 60. Starr TN, Greaney AJ, Hannon WW, Loes AN, Hauser K, Dillen JR, et al. Shifting
636 mutational constraints in the SARS-CoV-2 receptor-binding domain during viral
637 evolution. Science. 2022;377: 420–424. doi:10.1126/science.abo7896

638 61. Willett BJ, Grove J, MacLean OA, Wilkie C, De Lorenzo G, Furnon W, et al. SARS-CoV-2
639 Omicron is an immune escape variant with an altered cell entry pathway. Nat
640 Microbiol. 2022;7: 1161–1179. doi:10.1038/s41564-022-01143-7

641 62. Sun C, Xie C, Bu G-L, Zhong L-Y, Zeng M-S. Molecular characteristics, immune evasion,
642 and impact of SARS-CoV-2 variants. Sig Transduct Target Ther. 2022;7: 1–25.
643 doi:10.1038/s41392-022-01039-2

644 63. Kadam RU, Garg D, Schwartz J, Visini R, Sattler M, Stocker A, et al. CH−π "T-Shape"
645 Interaction with Histidine Explains Binding of Aromatic Galactosides to Pseudomonas
646 aeruginosa Lectin LecA. ACS Chem Biol. 2013;8: 1925–1930. doi:10.1021/cb400303w

647 64. Starr TN, Greaney AJ, Hilton SK, Ellis D, Crawford KHD, Dingens AS, et al. Deep
648 Mutational Scanning of SARS-CoV-2 Receptor Binding Domain Reveals Constraints on
649 Folding and ACE2 Binding. Cell. 2020;182: 1295-1310.e20.
650 doi:10.1016/j.cell.2020.08.012

651 65. Wang Q, Guo Y, Iketani S, Nair MS, Li Z, Mohri H, et al. Antibody evasion by SARS-CoV-2
652 Omicron subvariants BA.2.12.1, BA.4 and BA.5. Nature. 2022;608: 603–608.
653 doi:10.1038/s41586-022-05053-w

654 66. Han P, Su C, Zhang Y, Bai C, Zheng A, Qiao C, et al. Molecular insights into receptor
655 binding of recent emerging SARS-CoV-2 variants. Nat Commun. 2021;12: 6103.
656 doi:10.1038/s41467-021-26401-w

657 67. Mannar D, Saville JW, Zhu X, Srivastava SS, Berezuk AM, Tuttle KS, et al. SARS-CoV-2
658 Omicron variant: Antibody evasion and cryo-EM structure of spike protein–ACE2
659 complex. Science. 2022;375: 760–764. doi:10.1126/science.abn7760

660 68. Li L, Han P, Huang B, Xie Y, Li W, Zhang D, et al. Broader-species receptor binding and
661 structural bases of Omicron SARS-CoV-2 to both mouse and palm-civet ACE2s. Cell
662 Discov. 2022;8: 1–16. doi:10.1038/s41421-022-00431-0

663 69. Plowright RK, Parrish CR, McCallum H, Hudson PJ, Ko AI, Graham AL, et al. Pathways to
664 zoonotic spillover. Nat Rev Microbiol. 2017;15: 502–510. doi:10.1038/nrmicro.2017.45

665 70. Liu S, Selvaraj P, Sangare K, Luan B, Wang TT. Spike protein-independent attenuation of
666 SARS-CoV-2 Omicron variant in laboratory mice. Cell Reports. 2022;40: 111359.
667 doi:10.1016/j.celrep.2022.111359

668 71. Fenwick C, Turelli P, Perez L, Pellaton C, Esteves-Leuenberger L, Farina A, et al. A highly
669 potent antibody effective against SARS-CoV-2 variants of concern. Cell Reports.
670 2021;37: 109814. doi:10.1016/j.celrep.2021.109814

671 72. Fenwick C, Turelli P, Ni D, Perez L, Lau K, Herate C, et al. Patient-derived monoclonal
672 antibody neutralizes SARS-CoV-2 Omicron variants and confers full protection in
673 monkeys. Nat Microbiol. 2022;7: 1376–1389. doi:10.1038/s41564-022-01198-6

674 73. Fenwick C, Croxatto A, Coste AT, Pojer F, André C, Pellaton C, et al. Changes in SARS-
675 CoV-2 Spike versus Nucleoprotein Antibody Responses Impact the Estimates of
676 Infections in Population-Based Seroprevalence Studies. Journal of Virology. 2021;95:
677 e01828-20. doi:10.1128/JVI.01828-20

678 74. Punjani A, Rubinstein JL, Fleet DJ, Brubaker MA. cryoSPARC: algorithms for rapid
679 unsupervised cryo-EM structure determination. Nat Methods. 2017;14: 290–296.
680 doi:10.1038/nmeth.4169

681 75. Pettersen EF, Goddard TD, Huang CC, Couch GS, Greenblatt DM, Meng EC, et al. UCSF
682 Chimera—A visualization system for exploratory research and analysis. Journal of
683 Computational Chemistry. 2004;25: 1605–1612. doi:10.1002/jcc.20084

684 76. Emsley P, Lohkamp B, Scott WG, Cowtan K. Features and development of Coot. Acta
685 Cryst D. 2010;66: 486–501. doi:10.1107/S0907444910007493

686 77. Liebschner D, Afonine PV, Baker ML, Bunkóczi G, Chen VB, Croll TI, et al.
687 Macromolecular structure determination using X-rays, neutrons and electrons: recent
688 developments in Phenix. Acta Cryst D. 2019;75: 861–877.
689 doi:10.1107/S2059798319011471

690 78. Pettersen EF, Goddard TD, Huang CC, Meng EC, Couch GS, Croll TI, et al. UCSF ChimeraX:
691 Structure visualization for researchers, educators, and developers. Protein Science.
692 2021;30: 70–82. doi:10.1002/pro.3943

693

694 **Supporting Information**

695 **S1 Fig**: BLI assays of animal ACE2 against various variants of concern or mutants.

696 **S2 Fig:** Overview of the domain architecture of selected variants of concern. Mutations are
697 shown as red lines and labelled for each variant. Specific domains are highlighted: signal
698 peptide (SP), N- terminal domain (NTD), receptor binding domain (RBD), S1 and S2
699 domain.
700 **S3 Fig**: Cryo-EM processing of the mACE2/Beta complex
701 **S4 Fig**: Cryo-EM processing of the mACE2/BA.1 complex
702 **S5 Fig**: Cryo-EM processing of the mACE2/BA.2.12.1 complex
703 **S6 Fig**: Cryo-EM processing of the mACE2/BA.4/5 complex
704 **S7 Fig**: Cryo-EM processing of the hACE2/BA.4/5 complex
705 **S8 Fig**: FSC curves indicating resolutions at (FSC 0.143) and final focused refined maps
706 colored by local resolution.
707 **S9 Fig**: View of the 452 residue in various variants of concern with cryo-EM density.
708 **S10 Fig**: The BA.1 mutation Q493R abolishes interactions with the hACE2 residue K31
709 compared to wildtype.
710 **S1 Table**: Cryo-EM data collection and refinement statistics
711 **S1 Dataset**: BLI Raw data for Figure 1 and S1 Fig.
712

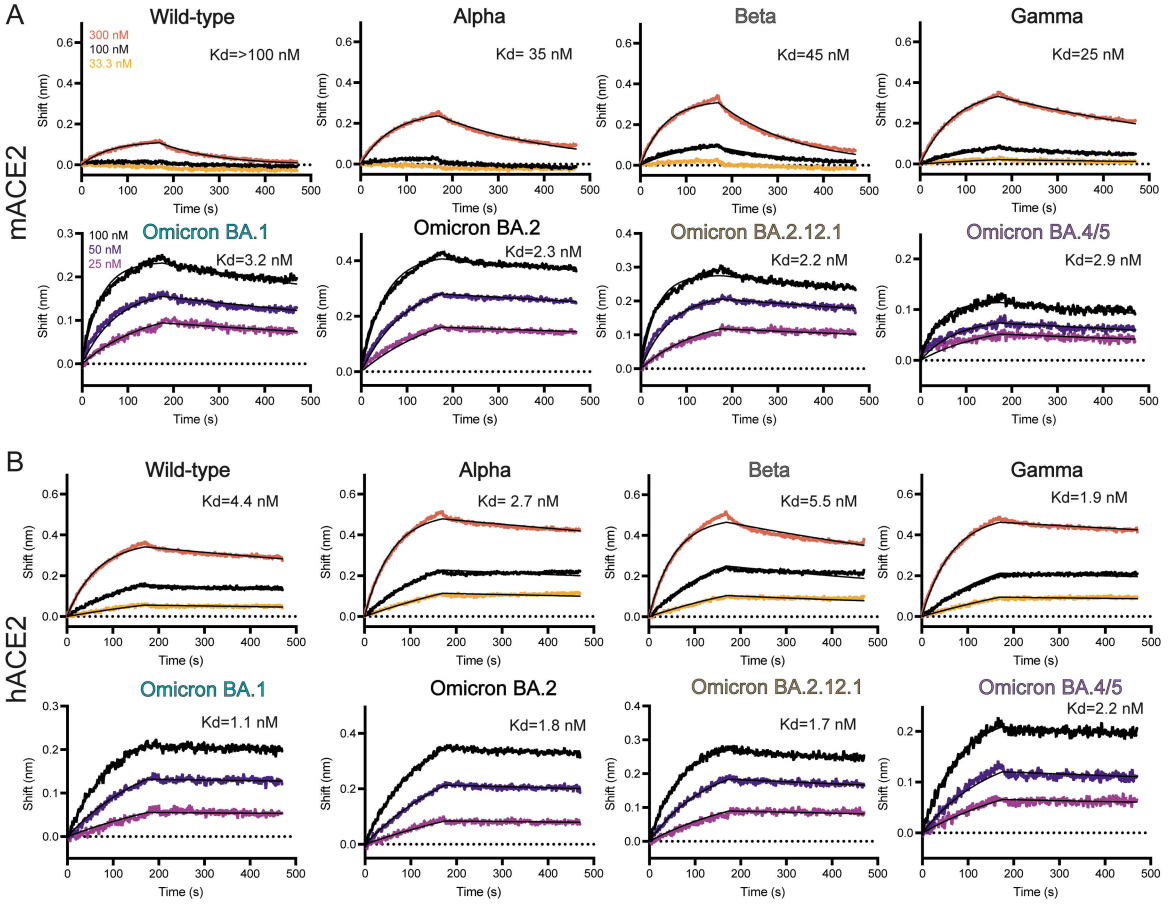

C

	19	24	27	28	30	31	34	35	37	38	41	42	45	79	82	83	330	353	355	357	393
human	S	Q	T	F	D	K	H	E	E	D	Y	Q	L	L	M	Y	N	K	D	R	R
mouse	S	N	T	F	N	N	Q	E	E	D	Y	Q	L	T	S	F	N	H	D	R	R
hamster	S	Q	T	F	D	K	Q	E	E	D	Y	Q	L	L	N	Y	N	K	D	R	R
cat	S	L	T	F	E	K	H	E	E	E	Y	Q	L	L	T	Y	N	K	D	R	R
dog	-	L	T	F	E	K	Y	E	E	E	Y	Q	L	L	T	Y	N	K	D	R	R
mink	S	L	T	F	E	K	Y	E	E	E	Y	Q	L	H	T	Y	N	K	D	R	R

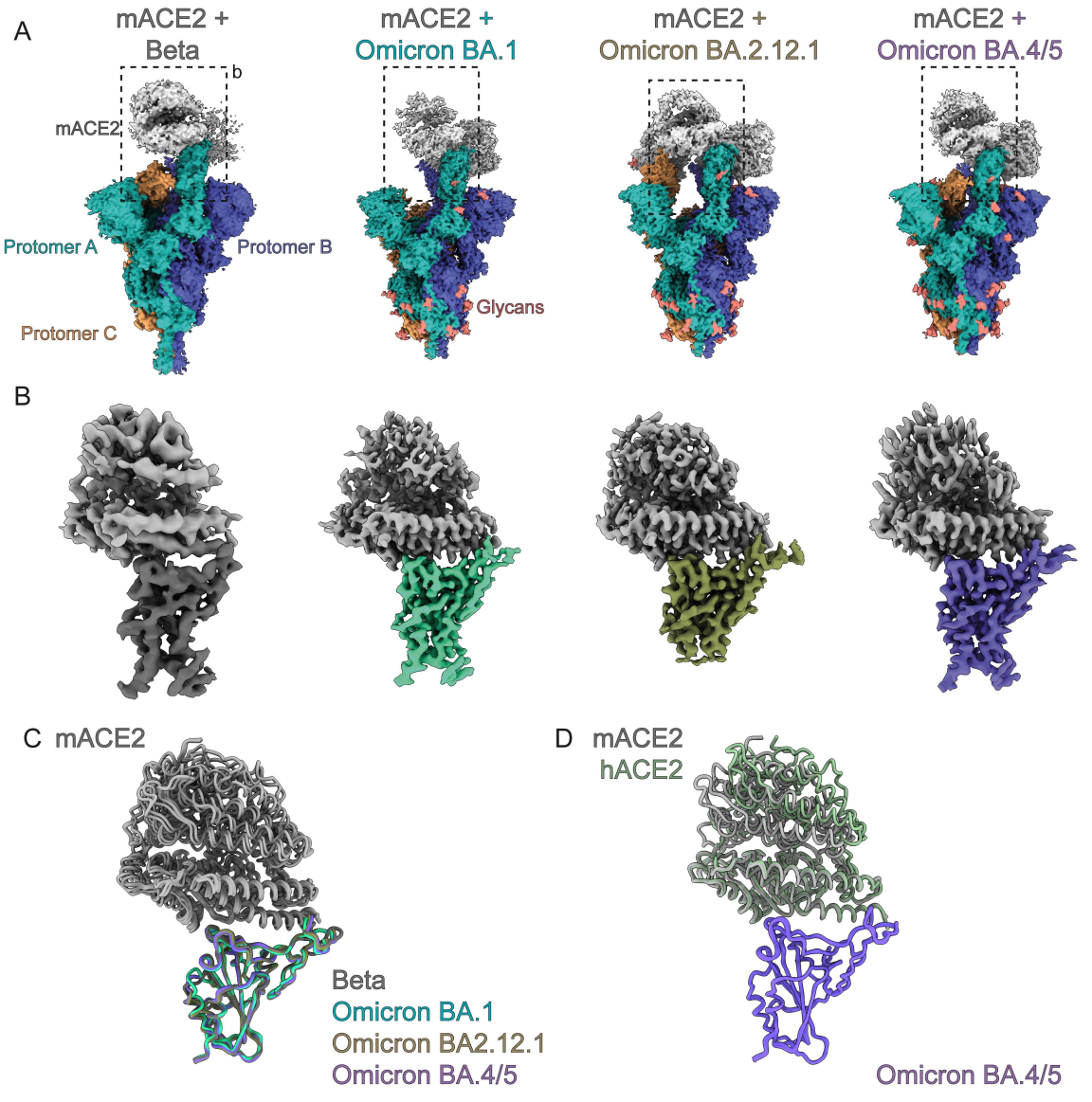
A
mACE2 +
Beta
mACE2 +
Omicron BA.1
mACE2 +
Omicron BA.2.12.1
mACE2 +
Omicron BA.4/5
b
mACE2
Protomer A
Protomer B
Protomer C
Glycans
B
C mACE2
Beta
Omicron BA.1
Omicron BA2.12.1
Omicron BA.4/5
D mACE2
hACE2
Omicron BA.4/5

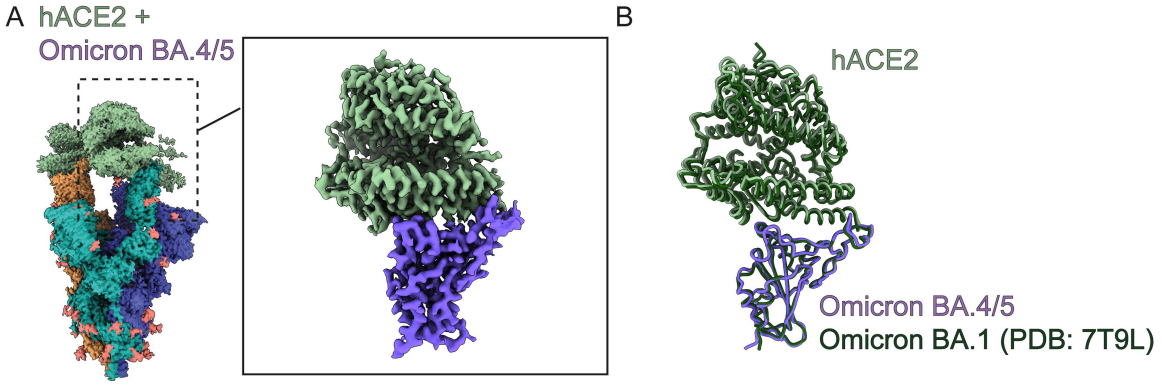
A
hACE2 +
Omicron BA.4/5
B
hACE2
Omicron BA.4/5
Omicron BA.1 (PDB: 7T9L)

A

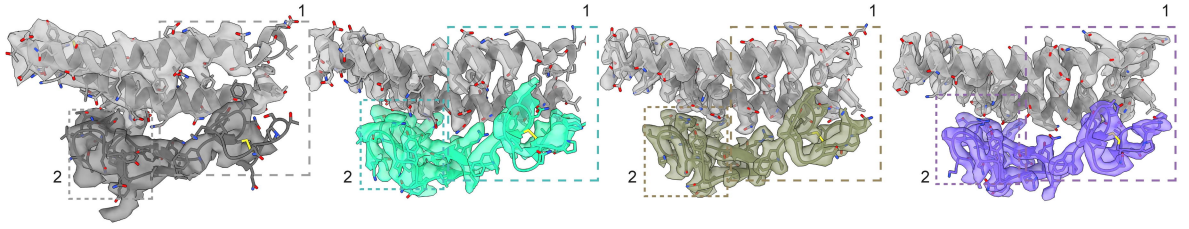

mACE2 + Beta | mACE2 + Omicron BA.1 | mACE2 + Omicron BA.2.12.1 | mACE2 + Omicron BA.4/5

B

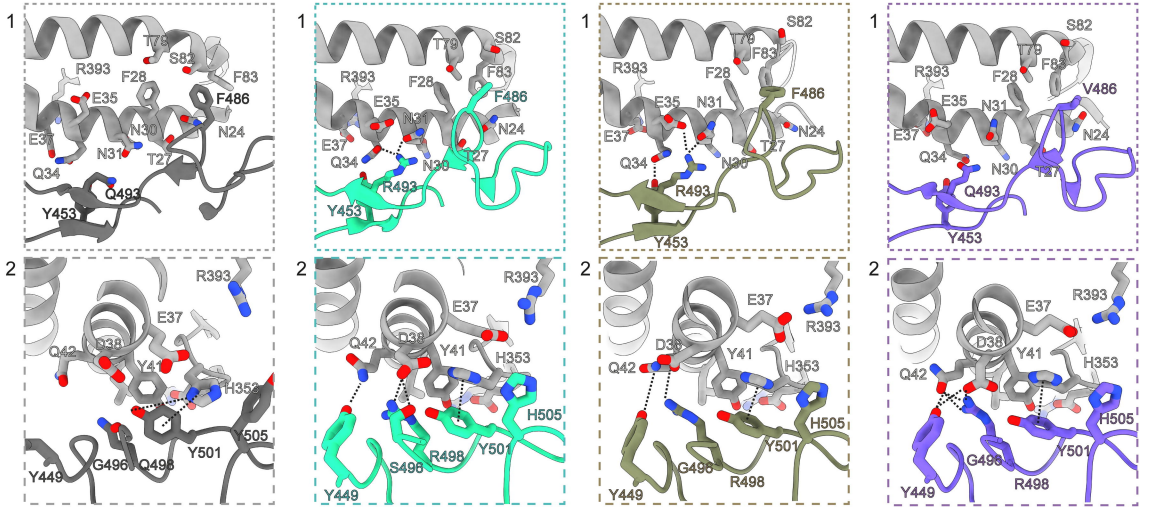

C
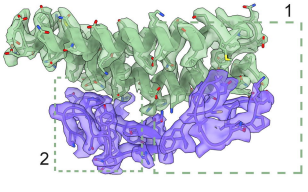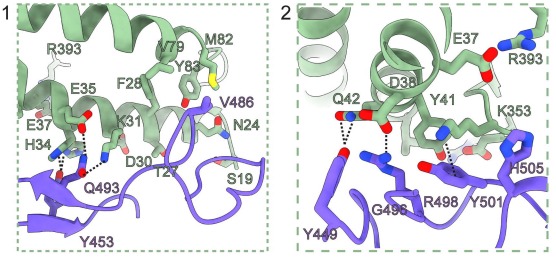
hACE2 + Omicron BA.4/5